



1 The effect of COVID-19 restrictions on atmospheric new particle formation 2 in Beijing

3
4 Chao Yan^{1,2,#}, Yicheng Shen^{3,#}, Dominik Stolzenburg², Lubna Dada^{2,4}, Ximeng Qi⁵, Simo
5 Hakala², Anu-Maija Sundström⁶, Yishuo Guo¹, Antti Lipponen⁷, Tom V. Kokkonen⁵, Jenni
6 Kontkanen², Runlong Cai^{2,3}, Jing Cai^{1,2}, Tommy Chan², Liangduo Chen⁵, Biwu Chu², Chenjuan
7 Deng³, Wei Du^{1,2}, Xiaolong Fan¹, Xu-Cheng He², Juha Kangasluoma^{1,2}, Joni Kujansuu^{1,2},
8 Mona Kurppa², Chang Li¹, Yiran Li³, Zhuohui Lin¹, Yiliang Liu⁸, Yuliang Liu⁵, Yiqun Lu⁸,
9 Wei Nie⁵, Jouni Pulliainen⁶, Xiaohui Qiao³, Yonghong Wang^{1,2}, Yifan Wen³, Ye Wu³, Gan
10 Yang⁸, Lei Yao², Rujing Yin³, Gen Zhang⁹, Shaojun Zhang³, Feixue Zheng¹, Ying Zhou¹, Antti
11 Arola⁷, Johanna Tamminen⁶, Pauli Paasonen², Yele Sun¹⁰, Lin Wang⁸, Neil M. Donahue¹¹,
12 Yongchun Liu¹, Federico Bianchi², Kaspar R. Daellenbach^{2,4}, Douglas R. Worsnop^{2,12}, Veli-
13 Matti Kerminen², Tuukka Petäjä^{2,5}, Aijun Ding^{5,*}, Jingkun Jiang^{3,*}, Markku Kulmala^{1,2,5*}

15 Affiliations:

16 ¹ Aerosol and Haze Laboratory, Beijing Advanced Innovation Center for Soft Matter Science and Engineering,
17 Beijing University of Chemical Technology, Beijing, China

18 ² Institute for Atmospheric and Earth System Research / Physics, Faculty of Science, University of Helsinki,
19 Finland

20 ³ State Key Joint Laboratory of Environment Simulation and Pollution Control, State Environmental Protection
21 Key Laboratory of Sources and Control of Air Pollution Complex, School of Environment, Tsinghua University,
22 Beijing, China

23 ⁴ Laboratory of Atmospheric Chemistry, Paul Scherrer Institute, 5232 Villigen, Switzerland.

24 ⁵ Joint International research Laboratory of Atmospheric and Earth System Research (JirLATEST), School of
25 Atmospheric Sciences, Nanjing University, Nanjing, China.

26 ⁶ Finnish Meteorological Institute, 00560 Helsinki, Finland

27 ⁷ Finnish Meteorological Institute, 70211 Kuopio, Finland

28 ⁸ Department of Environmental Science & Engineering, Fudan University, Shanghai, China

29 ⁹ State Key Laboratory of Severe Weather & Key Laboratory of Atmospheric Chemistry of China Meteorological
30 Administration (CMA), Chinese Academy of Meteorological Sciences, Beijing 100081, China

31 ¹⁰ Institute of Atmospheric Physics, Chinese Academy of Science, Beijing, China

32 ¹¹ Center for Atmospheric Particle Studies, Carnegie Mellon University, Pittsburgh, PA, USA

33 ¹² Aerodyne Research Inc., Billerica, Massachusetts 01821, USA

34 # these authors contributed equally to this work

35 * Correspondence to:

36 Markku Kulmala, markku.kulmala@helsinki.fi

37 Jingkun Jiang, jiangjk@tsinghua.edu.cn

38 Aijun Ding, dingaj@nju.edu.cn

39

40 Abstract

41 During the COVID-19 lockdown, the dramatic reduction of anthropogenic emissions provided
42 a unique opportunity to investigate the effects of reduced anthropogenic activity and primary
43 emissions on atmospheric chemical processes and the consequent formation of secondary
44 pollutants. Here, we utilize comprehensive observations to examine the response of
45 atmospheric new particle formation (NPF) to the changes in the atmospheric chemical cocktail.
46 We find that the main clustering process was unaffected by the drastically reduced traffic
47 emissions, and the formation rate of 1.5 nm particles remained unaltered. However, particle
48 survival probability was enhanced due to an increased particle growth rate (GR) during the



49 lockdown period, explaining the enhanced NPF activity in earlier studies. For GR at 1.5–3 nm,
50 sulfuric acid (SA) was the main contributor at high temperatures, whilst there were
51 unaccounted contributing vapors at low temperatures. For GR at 3–7 nm and 7–15 nm,
52 oxygenated organic molecules (OOMs) played a major role. Surprisingly, OOM composition
53 and volatility were insensitive to the large change of atmospheric NO_x concentration; instead
54 the associated high particle growth rates and high OOM concentration during the lockdown
55 period were mostly caused by the enhanced atmospheric oxidative capacity. Overall, our
56 findings suggest a limited role of traffic emissions in NPF.

57

58 1. Introduction

59 The pandemic of COVID-19 has led to the death of more than 5.3 million individuals
60 globally [WHO 2020, <https://covid19.who.int/>]. Restrictions on population movement
61 (lockdowns) worldwide led to arguably the most significant reduction of primary
62 anthropogenic emissions in recent history. NO_x concentrations declined on average by about
63 50 – 60 % in several European, South American, Indian, and Chinese cities (Sicard et al.,
64 2020; Krecl et al., 2020; Shi and Brasseur, 2020; Agarwal et al., 2020), and mixing ratios of other
65 primary pollutants, such as black carbon (BC), carbon monoxide (CO), sulfur dioxide (SO₂),
66 and volatile organic compounds (VOCs) were also reduced in varying degrees (Bao and Zhang,
67 2020; Chu et al., 2021; Shen et al., 2021b; Xing et al., 2020; Pei et al., 2020).

68 The reductions of primary emissions mitigated particulate pollution and improved air quality
69 in many countries around the globe (Sicard et al., 2020; Krecl et al., 2020; Agarwal et al., 2020;
70 Ciarelli et al., 2021), including many Chinese cities (Wang et al., 2020b; Huang et al., 2021;
71 Le et al., 2020). However, the reduction of PM_{2.5} was considerably weaker than those of the
72 primary pollutants, and in some cities such as Beijing, the PM_{2.5} concentrations even increased
73 after the lockdown policy was imposed (Huang et al., 2021). This persistent particulate
74 pollution has been attributed to both unfavorable meteorology, such as stagnant meteorological
75 conditions and high relative humidity (RH) (Le et al., 2020; Wang et al., 2020b) and to
76 enhanced atmospheric oxidative capacity caused by increased O₃ and NO₃ radical formation
77 (Huang et al., 2021; Le et al., 2020). To date, few studies have focused on either atmospheric
78 new particle formation or the overall particle number size distribution (Shen et al., 2021a; Shen
79 et al., 2021b) during the lockdown period, although NPF has been shown to enhance haze
80 formation (Guo et al., 2014; Kulmala et al., 2021), and the particle number size distribution is
81 known to influence the health effect of particles (Harrison et al., 2010).



82 NPF contains two consecutive stages: formation of particles via molecular clustering followed
83 by particle growth (Kulmala et al., 2014). A complete understanding of both stages remains
84 elusive in polluted urban environments. In the first stage, a key concern is the identity of the
85 clustering molecules. On one hand, several laboratory studies (Almeida et al., 2013; Xiao et
86 al., 2021) and ambient measurements (Yao et al., 2018; Yin et al., 2021; Yan et al., 2021; Cai
87 et al., 2021b; Deng et al., 2020) indicate that clustering between sulfuric acid (SA) and amines
88 drives the initial NPF in polluted environments. On the other hand, there are also studies
89 suggesting that organic acids formed from oxidation of traffic emissions are key clustering
90 species (Guo et al., 2020). The contrast between the enhanced NPF and reduced traffic load
91 during the lockdown period seems to support the former mechanism, but a detailed
92 investigation of how molecular clustering responded to those emission reductions remains
93 lacking. For the growth phase, oxygenated organic molecules (OOMs) have been shown to
94 dominate in some cases (Yan et al., 2021; Qiao et al., 2021). Further, a high fraction of nitrogen
95 containing OOMs suggests that RO_2+NO_x reactions prevail in OOM formation (Qiao et al.,
96 2021). For monoterpene-derived OOMs, which is characteristic of a remote atmosphere, high
97 NO_x levels can suppress particle growth by altering a fraction of products to organic nitrates
98 with higher volatilities (Yan et al., 2020). However, the effect of NO_x in OOM formation and
99 particle growth needs to be examined in urban settings, where the VOC precursors are largely
100 different.

101 Enhanced NPF during the lockdown period has been reported (Shen et al., 2021b), but without
102 a detailed explanation due to the lack of simultaneous measurements of both particles at the
103 size where NPF starts (e.g., 1.5 nm) and key vapors for NPF, such as SA and OOMs. We fill
104 that gap with comprehensive measurements from urban Beijing covering the lockdown period,
105 enabling the investigation on how NPF responded to the emission reductions during lockdown
106 on molecular and process levels.

107

108 **2. Methodology**

109 ***2.1 Measurement location and period***

110 The measurement campaign was conducted at the Aerosol and Haze Laboratory located at
111 the west campus of Beijing University of Chemical Technology (BUCT station, Lat. $39^\circ56'31''$
112 and Lon. $116^\circ17'52''$). It is a representative urban station surrounded by residential and
113 commercial areas and three main roads with heavy traffic loads. Measurements of atmospheric



114 variables and pollutants have been conducted continuously in this station since early 2018.
115 More details about the station and measurements can be found elsewhere (Liu et al., 2020).
116 The main data sets analyzed in this study were collected during 2019/12/15 – 2020/3/15,
117 divided into pre-lockdown (2019/12/15 - 2020/01/22) and lockdown (2020/01/23 – 2020/03/15)
118 periods. The Chinese Spring Festival (CSF) overlapped the lockdown period, but since they
119 have a similar effect on population movement, the CSF and COVID-19 periods were not
120 further separated in this study. As shown in Fig. S1-S3, the traffic congestion index, as well as
121 the NO₂ concentration measured by 11 national monitoring stations in Beijing and by satellite,
122 showed an apparent reduction and a slow rebound after the lockdown was imposed. In contrast,
123 traffic and the NO₂ concentration quickly rebounded after the CSF in 2019.

124

125 **2.2 Instrumentation**

126 The particle number size distribution over in the diameter range of 1 nm - 10 μm was
127 measured by the combination of a diethylene glycol scanning mobility particle spectrometer
128 (DEG-SMPS, 1-7.5 nm) and a particle size distribution system (PSD, 3 nm-10 μm). Particle
129 formation rates ($J_{1.5}$, J_3 , J_6 , and J_{10}) were calculated for all NPF cases using a new balance
130 formula that is optimized for polluted environments (Cai and Jiang, 2017). NPF is classified
131 according to the commonly-used criteria originally described by Dal Maso and co-workers
132 (Dal Maso et al., 2005), i.e., 1) a burst of sub-3 nm particles, and 2) continuous particle growth
133 in size. In some cases when only criterium 1 is satisfied, referred to as clustering events
134 hereafter, particle formation rates can still be calculated because growth is negligible compared
135 to coagulation and the dN/dt term for such small particles is in the formula. Hence, we included
136 both NPF events and clustering events when we investigated $J_{1.5}$, J_3 , and their response to other
137 relevant parameters. In addition, the condensation sink (CS) was calculated based on the
138 measurement of particle number size distribution (Kulmala et al., 2012). Detailed calculations
139 of particle formation rate and growth rate are provided in Supplementary Information (SI).

140 SA and OOM concentrations were measured with a nitrate ion-based Chemical Ionization
141 Atmospheric-Pressure-interface Long-Time-of-Flight mass spectrometer (CI-APi-LTOF,
142 Aerodyne Research, Inc.). The configuration of this instrument has been described previously
143 (Yan et al., 2021). Two levels of calibrations were performed. First, the SA concentration was
144 calibrated following the same procedure suggested by Kürten et al., (2012); Second, the mass-
145 dependent transmission efficiency of the instrument was obtained with the method developed



146 by Heintrizi et al., (2016). After these calibrations, the concentration of SA and OOMs can be
147 calculated using the equations below:

$$148 \quad [\text{SA}] = \frac{\text{HSO}_4^- + (\text{HNO}_3)\text{HSO}_4^-}{\sum_{i=0}^2 (\text{HNO}_3)_i \text{NO}_3^-} \times C \text{ Eq. (1)}$$

$$149 \quad [\text{OOM}] = \frac{(\text{OOM})\text{NO}_3^- + (\text{OOM}-\text{H})^-}{\sum_{i=0}^2 (\text{HNO}_3)_i \text{NO}_3^-} \times C \div T_{\text{OOM}} \text{ Eq. (2)}$$

150 In the righthand side of Eqs. 1 and 2, the numerator and denominator are the signals of analytes
151 and reagent ions, respectively, and C denotes the calibration coefficient obtained for SA, which
152 was determined as 7.0×10^9 (molecule·cm⁻³)/ncps. T_{OOM} in Eq.2 is the mass-dependent
153 transmission efficiency relative to the reagent ions.

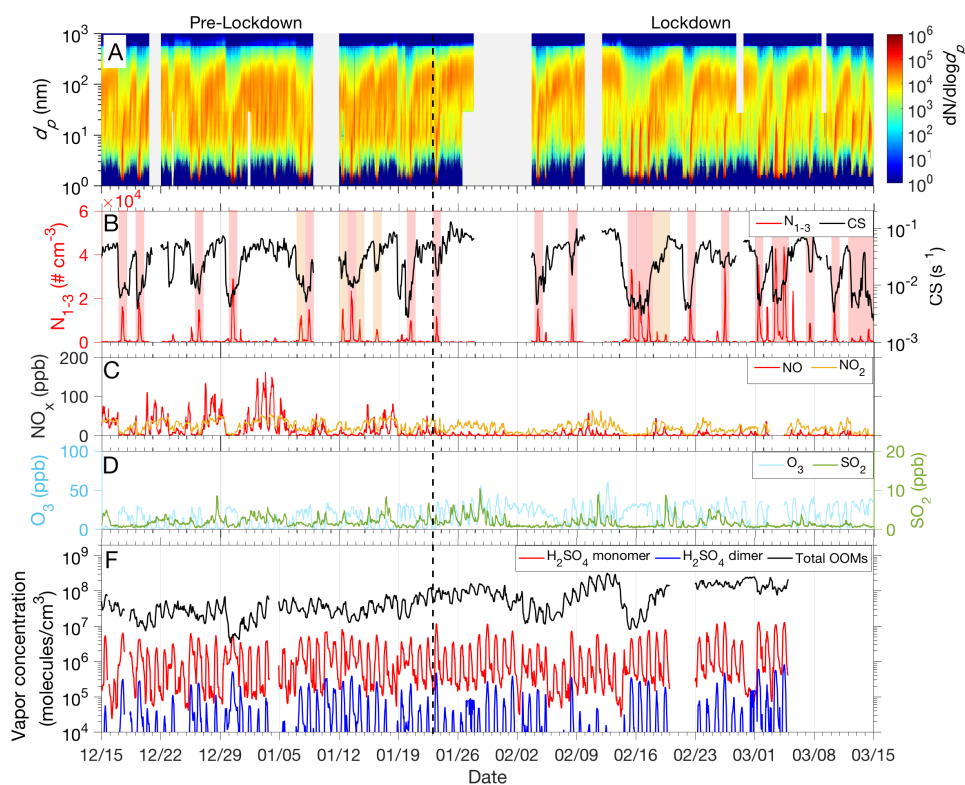
154 In addition, we measured the concentrations of CO, SO₂, NO_x, and O₃ using four Thermo
155 Environmental Instruments (models 48i, 43i-TLE, 42i, 49i, respectively). These trace-gas
156 pollutants were sampled through a 3-meter tube from the building roof, which was heated to
157 313 K to reduce sampling losses. Calibrations of these instruments were performed bi-weekly
158 using standard gases of known concentrations. In addition, several meteorological variables,
159 including the ambient temperature, relative humidity, pressure, visibility, UVB radiation, as
160 well as horizontal wind speed and direction, were measured with a weather station (AWS310,
161 Vaisala Inc.) located on the rooftop of the building. More details of these instruments are
162 provided in SI.

163

164 **3. Results and discussion**

165 ***3.1 Changes of atmospheric pollutants during the pre-lockdown and the lockdown periods***

166 We first investigated the extent to which lockdown restrictions modified pollution
167 concentrations. Figure 1 is an overview of the particle number size distributions and some
168 other relevant pollutants. As shown in Figure 1A&B, NPF occurred more frequently in the
169 lockdown period (30.8 %, 16 out of 52 days) than in the pre-lockdown period (18.0 %, 7 out
170 of 39 days). This difference is reduced if we include clustering events, to 34.6 % and 28.2 %
171 for the lockdown and pre-lockdown periods, respectively. Consistent with a few recent studies
172 (Cai et al., 2017; Yan et al., 2021; Deng et al., 2021), the burst in the concentration of sub-3
173 nm particles (N_{1-3} in Figure 1B) corresponded to a low CS during both periods, suggesting that
174 CS was the governing parameter for NPF.



175

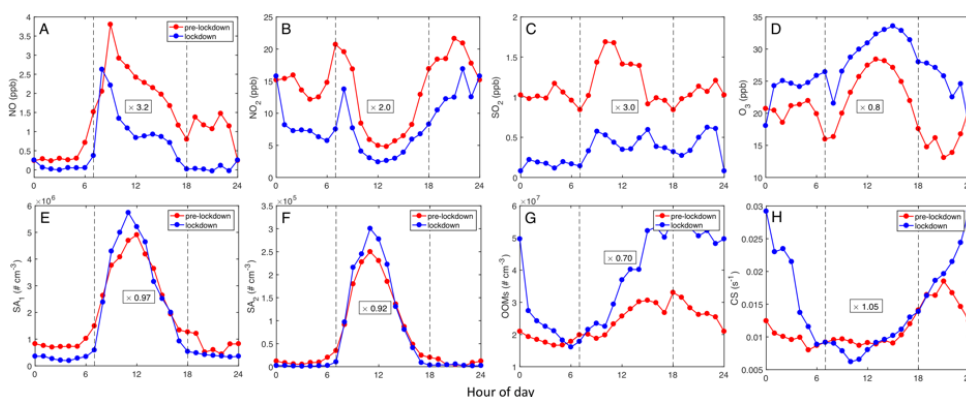
176 **Figure 1.** Concentrations of atmospheric pollutants during the pre-lockdown and lockdown periods,
177 including the particle number size distribution (A), number concentration of 1.5-3 nm particles (N_{1-3})
178 and NPF classification (B), NO and NO_2 (C), SO_2 and O_3 (D), and H_2SO_4 monomer, dimer, and total
179 oxygenated organic molecules (OOMs) (E). The vertical dashed line denotes the separation of the pre-
180 lockdown and the lockdown periods. In Panel B, days with NPF events and clustering events are shaded
181 in red and orange, respectively.

182

183 One prominent change of the particle number size distribution during the lockdown was
184 that particles in the size range of 10-30 nm were significantly reduced during the traffic rush
185 hours (Fig. S4), indicating that vehicle emissions contributed substantially to particles of this
186 size range during this time window. However, particles below this size range were not
187 substantially depleted, indicating a limited contribution of traffic emissions to the sub-10 nm
188 particle concentration in Beijing. This is in contrast to findings in some European countries
189 (Ronkko et al., 2017). A likely reason for this difference is that the observed NPF in Beijing
190 was notably more intense than in European cities, so it may have overwhelmed the contribution
191 of traffic emissions. Also, the abundant background aerosols in Beijing may have scavenged
192 any freshly-emitted particles more efficiently, so that fewer of these primary nano-particles
193 survived until observation.



194 Significant changes in the concentration of trace-gas pollutants coincided with the
195 lockdown. As shown in Figure 2A-C, NO, NO₂, and SO₂ concentrations during NPF periods
196 (7 am – 6 pm) decreased by 3.2-, 2.0-, and 3.0-fold (median values), respectively. As mentioned
197 above, the reduction of NO_x (NO_x=NO+NO₂) was directly related to the restriction of traffic.
198 However, the reduced SO₂ concentration was likely unrelated to the traffic restriction, because
199 the SO₂ concentrations did not exhibit a typical traffic pattern in either the pre-lockdown or the
200 lockdown period. Unlike the primary pollutants, O₃ concentrations increased by 25 % (Figure
201 2D), consistent with previous studies (Huang et al., 2021). Moreover, in comparison to the pre-
202 lockdown period, temperature and UVB radiation were higher during the lockdown period (Fig.
203 S5), suggesting stronger atmospheric photochemistry.



204

205 **Figure 2.** Median diurnal cycles of atmospheric variables during the pre-lockdown and lockdown
206 periods, including NO, NO₂, SO₂, O₃, SA₁, SA₂, OOMs, and CS. The ratio of $[X]_{\text{pre-lockdown}}/[X]_{\text{lockdown}}$ is
207 given in the framed text. Here, $[X]$ denotes the average value of a specific atmospheric variables during
208 the NPF time window, i.e., 7am – 6 pm, as marked by the two dashed lines.
209

210 The corresponding changes in the most NPF-relevant parameters, including sulfuric acid
211 monomers (SA₁), dimers (SA₂), oxygenated organic molecules (OOMs) and CS, are shown in
212 Figures 2E-H. The CS was almost identical between the pre-lockdown and lockdown periods
213 (Figure 2H). The median SA₁ and SA₂ concentrations were also stable between the two periods.
214 This is because the decline of the sulfuric acid precursor (i.e., SO₂, Figure 2C) was completely
215 compensated by the enhanced photochemistry, as indicated by the variation of UVB (Fig. S5B).
216 In addition, the concentration of OOMs increased by about 50% during the lockdown. This is
217 because the concentration of volatile organic compounds (VOCs) only declined slightly in the
218 lockdown period (Shen et al., 2021b), but the photochemistry was much more enhanced.

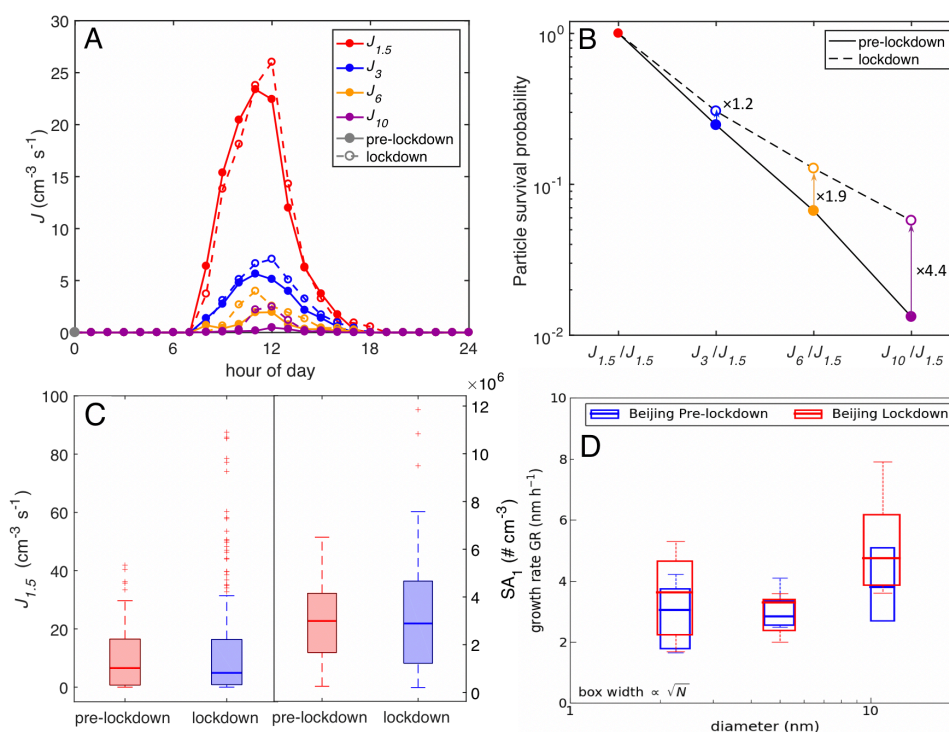
219 3.2 Changes in initial particle formation rate and size-segregated growth rates



220 Based on our previous studies of the governing factors and mechanism of NPF in Beijing
221 (Cai et al., 2017; Yan et al., 2021; Deng et al., 2021), we would expect the formation rates of
222 1.5 nm particles ($J_{1.5}$) during the two periods to be very similar because SA_1 , SA_2 , and CS were
223 nearly identical. However, this was not the case; a previous study in Beijing showed that NPF
224 was more intense during the lockdown period than in the pre-lockdown period (Shen et al.,
225 2021b). In order to resolve this puzzle, we examined the detailed formation rates calculated for
226 particles of different sizes, i.e., $J_{1.5}$, J_3 , J_6 , and J_{10} . We compare these formation rates in Figure
227 3A. Consistent with our initial expectation, $J_{1.5}$ was very similar in these two periods; however,
228 at progressively larger particle sizes the difference of particle formation rates during the two
229 periods becomes progressively more pronounced. This means that, while the nucleation rates
230 remained constant, more of the newly formed particles survived during the lockdown period.
231 As shown in Figure 3B, the particle survival probabilities, calculated as J_{dp2}/J_{dp1} from 1.5 nm
232 to 3 nm, 6 nm, and 10 nm during the lockdown period were enhanced by factors of 1.2, 1.9 and
233 4.4, respectively, compared to pre-lockdown conditions. This provides one explanation for the
234 enhanced particle formation rates reported previously – if the particles were only measured at
235 a size larger than 1.5 nm, the calculated formation rate would be larger in the lockdown period
236 due to the enhanced particle survival probability. In addition, despite the similar median values
237 of $J_{1.5}$, a few intense NPF cases occurred during the lockdown period, in contrast to the pre-
238 lockdown period (Figure 3C). In such cases, the classification of NPF events, which is to some
239 extent subjective, could also affect the comparison (a classification bias). For instance, if weak
240 NPF events were not detected or counted, the average $J_{1.5}$ during the lockdown period would
241 be higher. This could be another reason for the reported stronger NPF in the lockdown period
242 (Shen et al., 2021b).



243



244

245 **Figure 3.** The diurnal cycles of particle formation rates, growth rates, and survival probability (median
 246 values) at different sizes during the pre-lockdown and lockdown periods. (A) diurnal variations of
 247 particle formation rates at different sizes, i.e., J_1 , J_3 , J_6 and J_{10} . (B) Particle survival probability as a
 248 function of size. (C) Box plots showing the distribution of $J_{1.5}$ and SA_1 . (D) Size-segregated particle
 249 growth rates.
 250

251 The particle survival probability is mostly determined by the competition between particle
 252 growth and scavenging by pre-existing large particles (Kerminen and Kulmala, 2002; Lehtinen
 253 et al., 2007). As the scavenging rate of nanoparticles is approximately proportional to CS , the
 254 particle survival probability is proportional to the ratio of particle growth rate (GR) to CS
 255 (GR/CS) (Kulmala et al., 2017). In our observations, CS values during the time windows of
 256 NPF events were similar in these two periods (Figure 2H), so a change in GR must be the key
 257 to the different particle survival probability. To explore this, we calculated size-dependent
 258 growth rates of sub-10 nm particles in the pre-lockdown and lockdown periods with the
 259 appearance-time method. This method gives a higher GR than the mode-fitting method (Deng
 260 et al., 2020; Qiao et al., 2021). Consistent with previous studies (Deng et al., 2020; Qiao et al.,
 261 2021), larger particles had higher growth rates (Figure 3D). The reason for the enhanced
 262 particle growth will be discussed in detail in Section 3.4.



263

264 ***3.3 Insights into the clustering mechanism and its response to the lockdown conditions***

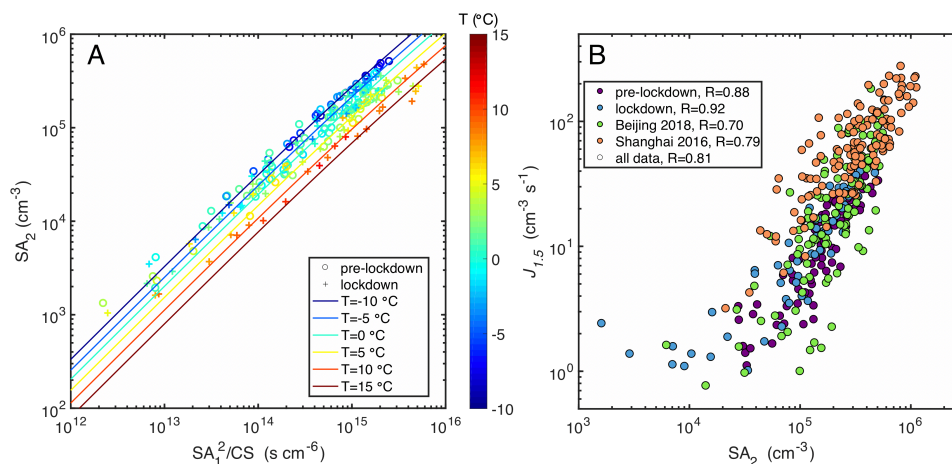
265 An important conclusion from our observations is that the clustering efficiency was not
266 significantly affected by the lockdown restrictions, as otherwise, $J_{1.5}$ would have most likely
267 changed drastically even though the SA concentration and CS were identical. For example, it
268 has been shown that particle formation rates differ by up to a factor of 1000 when SA clusters
269 with dimethylamine (DMA) instead of ammonia (Almeida et al., 2013), for constant SA and
270 CS. Hence, we further investigated the clustering efficiency of SA and the relationship between
271 SA_2 and $J_{1.5}$, focusing on comparisons between the pre-lockdown and lockdown periods.

272 An important diagnostic of SA clustering is the efficiency of SA_2 formation via the collision
273 of two SA_1 . Here, SA_1 and SA_2 denote monomers and dimers of SA, which may also contain
274 base molecules acting as the stabilizer. Those base molecules cannot be seen by the nitrate-CI-
275 APi-TOF because of their evaporation during charging processes or inside the instrument
276 (Kurten et al., 2014). As the stabilizing effect of amines is much stronger than that of ammonia,
277 SA_2 formation efficiency is notably higher in the SA-amine system than in the SA-ammonia
278 system (Almeida et al., 2013; Kurten et al., 2014). In addition, the SA_2 formation efficiency
279 also depends on the concentration of base molecules, CS, as well as on the temperature (Cai et
280 al., 2021a). As shown in Figure 4, the most prominent feature of the SA_2 formation efficiency
281 in our observations is a clear dependence on temperature; SA_2 concentrations were consistently
282 lower at higher temperatures. This dependence was identical for both the pre-lockdown and
283 lockdown periods. On the other hand, the clustering efficiency appears to be independent of
284 CS, because the loss of SA_1 -DMA₁ clusters was dominated by evaporation over the
285 temperature range of our observations (Fig. S6).

286 With a simplified SA-DMA clustering approach (Cai et al., 2021a), we were able to
287 reproduce the SA_2 formation, including its temperature dependence. Since the clustering
288 efficiency was not affected by CS, we set $CS=0.01\text{ s}^{-1}$ for the simulations. For that CS, the best
289 simulation result was obtained when the DMA concentration was constant at 1.3 ppt with a
290 50 % uncertainty, showing no systematic difference between the pre-lockdown and lockdown
291 periods (Fig. S7). This is less than the measured DMA concentration in 2018 in Beijing (Deng
292 et al., 2020). It should be noted that this effective DMA concentration (i.e., 1 ppt) is not the
293 “real” concentration of DMA, but rather it means that the stabilizing effect of all base
294 molecules is equivalent to that of 1 ppt DMA.



295



296

297 **Figure 4.** Clustering of SA and formation of new particles during the pre-lockdown and lockdown
298 periods. (A) Measured daytime (7 am – 6 pm) SA_2 (dimer) concentration versus squared SA_1
299 concentration divided by CS, color-coded by temperature. This represents the dimer production
300 efficiency. Lines denote clustering model simulations(Cai et al., 2021a). The simulations deployed a
301 constant dimethylamine concentration (1 ppt) and CS (0.01 s^{-1}), which provided the best agreement
302 with the ambient measurements. (B) Measured particle formation rate $J_{1.5}$ versus SA_2 concentration
303 color-coded by different datasets. Measurements in 2018 wintertime Beijing (Yan et al., 2021) and in
304 Shanghai (Yao et al., 2018) are also included. It should be noted that, $J_{1.7}$ was used in the study in
305 Shanghai.
306

307 As shown in Figure 4B, $J_{1.5}$ correlates well with the SA_2 concentration, indicating that particle
308 formation is driven by SA clustering processes. The relationship between $J_{1.5}$ and the SA_2
309 concentration agrees well with earlier observations in Beijing (Yan et al., 2021) and Shanghai
310 (Yao et al., 2018), with a correlation coefficient of 0.81 for all data. However, in comparison
311 to those earlier studies, $J_{1.5}$ in our observations is slightly lower, which could be attributed to
312 the lower DMA concentration as discussed above. Most importantly, Figure 4A and 4B clearly
313 indicate that the mechanisms of both SA clustering and initial particle formation remained the
314 same in the pre-lockdown and lockdown periods, although a clear temperature effect can be
315 seen. This gives direct evidence that the gaseous species emitted by traffic exhaust and their
316 associated photochemical products alone are not the main source of either sulfuric acid or new
317 particles in Beijing.

318

319 **3.4 Characteristics of oxygenated organic molecules and the contribution to particle growth**

320 Particle growth is key to particle survival, and subsequently the climate and health effects.
321 Therefore, it is essential to understand the vapors responsible for particle growth, as well as the
322 reason why particle growth was enhanced during the lockdown period, in spite of reduced



323 primary emissions. As the sulfuric acid concentration remained stable (Figure 2E) and it had a
324 minor contribution to the growth of particles larger than 3 nm (Deng et al., 2020; Qiao et al.,
325 2021), the enhanced particle growth rates were more likely associated with corresponding
326 changes of OOMs than sulfuric acid.

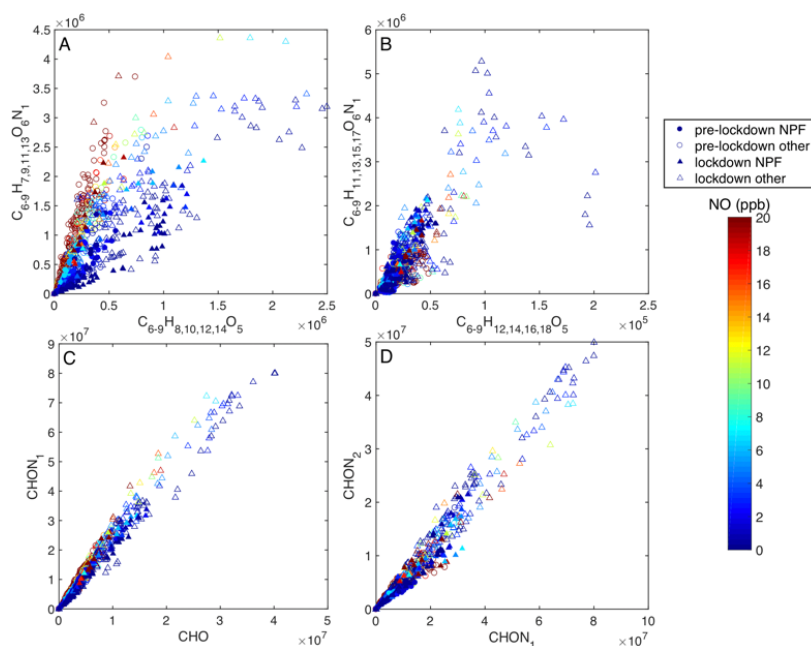
327 Recent studies have suggested that elevated NO_x can suppress the formation of low-
328 volatility vapors by inhibiting the autoxidation of RO_2 radicals (Yan et al., 2020). Due to the
329 significant NO_x reductions during the lockdown period, pronounced changes in OOM
330 composition were expected. Such changes were indeed observed for some OOMs. For instance,
331 as shown in Figure 5A, the ratio between two indicative compound categories varied
332 significantly as a function of NO. Here, the categories $\text{C}_{6-9}\text{H}_{7,9,11,13}\text{O}_6\text{N}$ and $\text{C}_{6-9}\text{H}_{8,10,12,14}\text{O}_5$ are
333 the termination products of bicyclic peroxy radicals originating from aromatics ($\text{C}_{6-9}\text{H}_{7,9,11,13}\text{O}_5$)
334 (Wang et al., 2017) formed through reactions with NO and HO_2 , respectively. When the NO
335 concentration declined from the pre-lockdown period to the lockdown period, the ratio of C_{6-9} -
336 $\text{H}_{7,9,11,13}\text{O}_6\text{N}$ concentration to $\text{C}_{6-9}\text{H}_{8,10,12,14}\text{O}_5$ concentration decreased as well.

337 However, the majority of OOMs were insensitive to the declining NO. For example, the
338 ratio of categories $\text{C}_{6-9}\text{H}_{11,13,15,17}\text{O}_6\text{N}$ and $\text{C}_{6-9}\text{H}_{12,14,16,18}\text{O}_5$ did not depend on the NO
339 concentration (Figure 5B). These compounds are presumably termination products of C_{6-9} -
340 $\text{H}_{11,13,15,17}\text{O}_4$ radicals through reactions with NO and HO_2 , respectively. They have a double
341 bond equivalent (DBE) of 1, suggesting that they originate from aliphatic rather than aromatic
342 precursors. Their NO_x sensitivity differs from the OOMs derived from aromatics. It could be
343 that even at low NO_x concentrations, the reaction with NO is necessary to form OOMs from
344 these peroxy radicals, as nitrogen-containing OOMs were consistently far more abundant than
345 nitrogen-free OOMs. Figure 5C and 5D also show that the overall nitrogen number of OOMs
346 did not depend on NO.

347 The overall OOM composition was surprisingly insensitive to changes in NO_x
348 concentrations. OOM chemical characteristics, i.e., the distributions of carbon number, oxygen
349 number, nitrogen number, hydrogen number, hydrogen-to-carbon ratio, and oxygen-to-carbon
350 ratio, remained almost identical during the two periods (Fig. S8). The stable OOM composition
351 indicates similar “intrinsic” (300 K) volatility distributions in the pre-lockdown and lockdown
352 periods, as shown in Figure S8. The mean temperatures were about 274 K and 280 K in these
353 periods, respectively (Figure S4A), and as a result, the ambient-temperature OOM volatilities
354 were both lower than the intrinsic values but similar to each other due to the small temperature
355 difference (Fig. S9). Therefore, we conclude that the influences of both temperature and
356 RO_2+NO_x chemistry on OOM vapor condensation and the resulting particle growth rates were



357 very small. Though the OOM volatility distribution was stable between the pre-lockdown and
358 lockdown periods, the OOM concentrations increased during the lockdown period, likely due
359 to enhanced photochemistry.
360



361
362 **Figure 5.** The influence of NO (given by symbol color) on the composition of OOMs, indicated by the
363 ratio between nitrogen-containing and nitrogen-free OOMs. (A) Selected OOMs with a double-bond-
364 equivalent (DBE) of 3, which are usually products from the oxidation of aromatic compounds (Molteni
365 et al., 2018; Wang et al., 2017; Garmash et al., 2020). (B) Selected OOMs with a DBE of 1, which are
366 more likely formed from the oxidation of aliphatic compounds, such as alkenes and alkanes. (C) OOMs
367 containing 0 and 1 nitrogen atom. (D) OOMs containing 1 and 2 nitrogen atoms. In all panels, only
368 daytime data (7:00 – 18:00) were included as they are directly relevant to NPF. Circles and triangles
369 represent data in pre-lockdown and lockdown periods, respectively; filled and empty markers denote
370 data during NPF days and other days, respectively.

371
372 Next, we examine contributions of SA and OOM to observed GRs in different size ranges,
373 i.e., 1.5 – 3 nm (GR_{1.5-3}), 3 – 7 nm (GR₃₋₇), and 7 – 15 nm (GR₇₋₁₅). Overall, this shows that
374 different processes govern growth at different sizes and temperatures.

375 Sulfuric acid contributed a relatively constant 1-1.5 nm/h to GR_{1.5-3} as shown in Figure
376 6A. At high temperatures ($T > 0$ °C) this explains most of the growth. However, at low
377 temperatures ($T < 0$ °C), SA condensation alone does not explain the observed GR₁₋₃,
378 suggesting an important contribution of other vapors favored by low temperatures. The vapors
379 and processes responsible for the residual GR_{1.5-3} remain unclear, but they do not appear to be
380 OOMs, since the residual GR_{1.5-3} ($GR_{\text{measured}} - GR_{\text{SA}}$) after subtracting SA contribution does



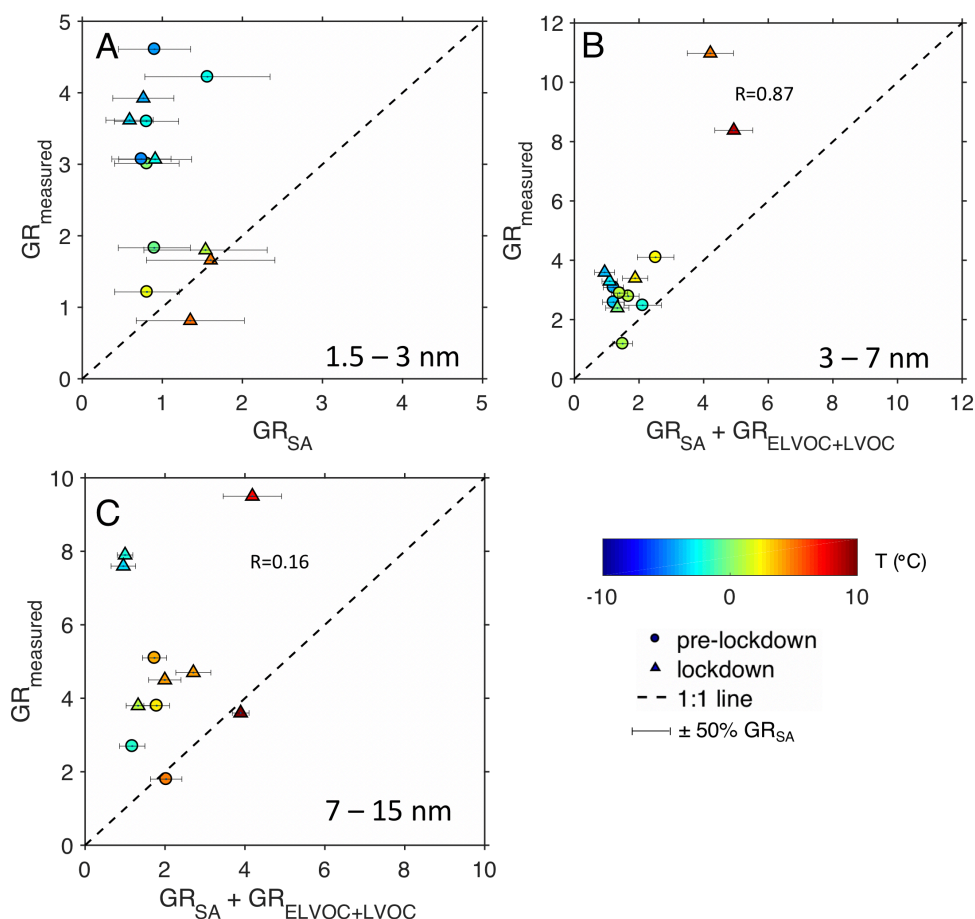
381 not show a positive correlation with condensable OOM concentration (Fig. S10). In fact, the
382 residual GR_{1-3} shows a negative correlation with OOM concentration, mainly because of the
383 coincidence of high OOM concentration and high temperature. One possibility could be the
384 co-condensation of nitric acid and ammonia at low temperatures, as recently reported in
385 controlled chamber experiments (Wang et al., 2020a). However, observational evidence is
386 required to verify this hypothesis.

387 Above 3 nm, the growth rate from sulfuric acid condensation drops well below 1 nm/h, and
388 condensation from observed OOMs explains 1-4 nm/h of additional growth. For GR_{3-7} the
389 OOM condensation correlates well with the observed GR ($R=0.87$) but the calculated GR was
390 lower than the observed value by roughly a factor of 2. The largest observed and calculated
391 growth was at the highest temperature during the lockdown, suggesting more efficient
392 photochemical production, though a residual excess at lower temperature may be related to
393 nitric acid and ammonia condensation. The correlation between calculated and observed
394 growth degrades for GR_{7-15} , though the highest observed and calculated values continue to be
395 at higher temperature. Given the growth rates, these particles are several hours old, and so
396 urban inhomogeneity may degrade this local analysis.

397 In laboratory experiments for growth by condensation of terpene oxidation products it has been
398 shown that the nitrate cluster ionization can miss up to half of the condensable organic vapors
399 (Trostl et al., 2016; Stolzenburg et al., 2018), and this could be true as well for these urban
400 conditions. If we scale the measured OOM concentrations with the same factors used by Tröstl
401 et al., (Trostl et al., 2016) (see SI), the measured and calculated GR fall close to the one-to-one
402 line (Fig. S10). Hence, underestimated OOM concentrations may well explain the under
403 predictions above 3 nm, although other possible reasons cannot be fully excluded, for instance,
404 the contribution of multiphase chemistry.



405



406

407 **Figure 6.** Connections of size-segregated particle growth rates to the plausible vapor concentrations.
408 (A). The observed $GR_{1.5-3}$ versus the $GR_{1.5-3}$ predicted with SA. (B). GR_{3-7} versus the predicted GR
409 considering SA and condensable OOMs (the sum of ULVOC, ELVOC, and LVOC, see SI). (C). GR_{7-15}
410 versus the predicted GR considering SA and condensable OOMs. The contribution of SA to particle
411 growth is estimated using the equation by Stolzenburg et al., (Stolzenburg et al., 2020) and the
412 contribution of condensable OOM was calculated assuming ELVOC and LVOC were effectively non-
413 volatile (Nieminen et al., 2010; Ehn et al., 2014). The measurement uncertainty ($\pm 50\%$) of SA (Kurten
414 et al., 2012) is shown as the horizontal error bars. All plots are color-coded with the mean temperature
415 at the corresponding time window. The linear correlation coefficients between the measured and
416 calculated GRs in Panel B and C are also given.

417

418 4. Summary and Atmospheric implications

419 We examined the response of NPF to emission reductions in Beijing during the COVID-19
420 lockdown in both the molecular and the process levels. Clustering between SA and other base
421 molecules drove the initial NPF in both pre-lockdown and lockdown periods. Our results show



422 that this clustering was insensitive to the emission reductions. However, it is evident that the
423 clustering efficiency of SA declined at high temperatures. This provides direct observational
424 evidence that traffic emissions alone cannot be a major source of NPF in Beijing, in contrast
425 to a few recent studies in urban areas (Ronkko et al., 2017; Guo et al., 2020).

426 The lockdown period showed an enhanced atmospheric oxidative capacity and reduced SO₂
427 concentrations; these balanced, so that both the SA concentration and particle formation rates
428 at 1.5 nm ($J_{1.5}$) were similar during the pre-lockdown and lockdown periods. This appears to
429 contradict a prior study reporting that NPF became stronger during the lockdown period based
430 on a measurement of particles down to 2 nm (Shen et al., 2021b). However, this apparent
431 discrepancy is mainly due to an increased particle survival probability caused by enhanced
432 particle growth during the lockdown period. To disentangle particle formation and growth,
433 measurement of particles at or below 1.5 nm is crucial to understanding the formation
434 mechanism of new particles.

435 The most obvious reason for the greater particle growth during the lockdown period was
436 elevated OOM concentrations due to enhanced photochemistry. We also expected that lower
437 NO_x would favor particle growth, as NO can suppress particle growth by altering the OOM
438 composition and increasing the overall OOM volatility (Yan et al., 2020). This turned out not
439 to be the case in our study. We observed some changes in OOM composition in molecules
440 derived from oxidation of aromatic VOCs, but for the most part changes in OOM composition
441 and volatility were negligible. This suggests that the RO₂ + NO reaction remains important to
442 OOM formation even after such a dramatic NO_x reduction. It has been proposed that
443 atmospheric RO₂ autoxidation will be increasingly more important if NO_x keeps declining in
444 North America (Praske et al., 2018), which might potentially enhance peroxide-driven particle
445 toxicity and the yield of secondary organic aerosol (Zhao et al., 2017). However, our results
446 suggest that these adverse effects on human health and air quality are less likely to occur in
447 Beijing, at least in the near future.

448 A crucial challenge is to understand the key vapors and processes determining particle growth
449 rates. We investigated particle growth over three consecutive size ranges: 1.5 – 3 nm, 3 – 7 nm,
450 and 7 – 15 nm. Particle growth in each range shows distinct features and its relationship with
451 condensable vapors is the same in both periods. SA condensation almost completely explains
452 GR_{1.5-3} at high temperatures. The co-condensation of nitric acid and ammonia might be an
453 important contributor at low temperatures, but this needs further verification by observations.
454 Condensation of OOMs plays a dominant role above 3 nm. Measured GR₃₋₇ and OOMs are
455 highly correlated. After scaling measured OOMs (by approximately a factor of 2) to account



456 for compounds that escape detection by NO_3^- chemical ionization, the calculated GR_{3-7} and
457 GR_{7-15} match the observed growth rates. The correlation with observations degrades at the
458 larger size range, where particles are several hours old; there may be complex influences by
459 other processes, such as the urban micro-meteorology and air mass inhomogeneity, which
460 warrant future investigation.

461

462 Acknowledgements

463 National Key R&D Program of China (2019YFC0214701, 2017YFC0209503,
464 2016YFC0200500), National Natural Science Foundation of China (41877306, 21876094) and
465 Samsung PM2.5 SRP. All co-authors acknowledge the support of Beijing University of
466 Chemical Technology. This work was supported by the Academy of Finland (1251427,
467 1139656, 296628, 306853, 316114, and 311932) & Finnish centre of excellence 1141135 &
468 307331, the EC Seventh Framework Program and European Union's Horizon 2020 program
469 (ERC, project no.742206 "ATM-GTP", no. 850614 "CHAPAs"), the European Union's
470 Horizon 2020 research and innovation programme under the Marie Skłodowska-Curie grant
471 agreement No 895875 ("NPF-PANDA"), European Regional Development Fund, Urban
472 innovative actions initiative (HOPE; Healthy Outdoor Premises for Everyone, project nro:
473 UIA03-240), MegaSense by Business Finland (Grant 7517/31/2018), trans-national ERA-
474 PLANET project SMURBS (Grant Agreement 689,443) under the EU Horizon 2020
475 Framework Programme, and Academy of Finland Flagship funding (grant no. 337549) is
476 gratefully acknowledged. Centre of Excellence in Inverse Modeling and Imaging, Academy of
477 Finland project 312125 is acknowledged. Kaspar R. Daellenbach received support from the
478 Swiss National Science postdoc mobility grant (P2EZIP2_18159). Juha Kangasluoma received
479 funding from UHEL 3-year grant (75284132), Finnish Academy of Science project (1325656).
480 Simo Hakala and Mona Kurppa acknowledge the doctoral programme in atmospheric sciences
481 (ATM-DP, University of Helsinki). Neil Donahue acknowledges the US NSF (grant
482 AGS1801897). Aijun Ding acknowledges the national natural science foundation of China
483 (41725020). Lin Wang acknowledges the national natural science foundation of China
484 (91644213, 21925601).

485

486 **Author contributions:** CY, YS, AD, JJ, and MK. designed the study; CY, YS, XQ, AMS,
487 YG, LC, CD, ZL, and FZ conducted the measurement or collected key materials; CY, YS,
488 XQ, LD, DS, SH, AMS, YG, TK, and JK analyzed the data; CY wrote the manuscript; all
489 coauthors have read and commented on the manuscript.

490 **Competing interests:** The authors declare no competing interest.

491 **Data and materials availability:** Data and materials are available upon contacting the
492 corresponding authors

493

494 References

495

496 Agarwal, A., Kaushik, A., Kumar, S., and Mishra, R. K.: Comparative study on air quality
497 status in Indian and Chinese cities before and during the COVID-19 lockdown period, Air
498 Quality, Atmosphere & Health, 1-12, 10.1007/s11869-020-00881-z, 2020.



- 499 Almeida, J., Schobesberger, S., Kurten, A., Ortega, I. K., Kupiainen-Maatta, O., Praplan, A.
500 P., Adamov, A., Amorim, A., Bianchi, F., Breitenlechner, M., David, A., Dommen, J.,
501 Donahue, N. M., Downard, A., Dunne, E., Duplissy, J., Ehrhart, S., Flagan, R. C., Franchin,
502 A., Guida, R., Hakala, J., Hansel, A., Heinritzi, M., Henschel, H., Jokinen, T., Junninen, H.,
503 Kajos, M., Kangasluoma, J., Keskinen, H., Kupc, A., Kurten, T., Kvashin, A. N., Laaksonen,
504 A., Lehtipalo, K., Leiminger, M., Leppa, J., Loukonen, V., Makhmutov, V., Mathot, S.,
505 McGrath, M. J., Nieminen, T., Olenius, T., Onnela, A., Petaja, T., Riccobono, F., Riipinen, I.,
506 Rissanen, M., Rondo, L., Ruuskanen, T., Santos, F. D., Sarnela, N., Schallhart, S.,
507 Schnitzhofer, R., Seinfeld, J. H., Simon, M., Sipila, M., Stozhkov, Y., Stratmann, F., Tome,
508 A., Trostl, J., Tsagkogeorgas, G., Vaattovaara, P., Viisanen, Y., Virtanen, A., Vrtala, A.,
509 Wagner, P. E., Weingartner, E., Wex, H., Williamson, C., Wimmer, D., Ye, P., Yli-Juuti, T.,
510 Carslaw, K. S., Kulmala, M., Curtius, J., Baltensperger, U., Worsnop, D. R., Vehkamäki, H.,
511 and Kirkby, J.: Molecular understanding of sulphuric acid-amine particle nucleation in the
512 atmosphere, *Nature*, 502, 359-363, 10.1038/nature12663, 2013.
- 513 Bao, R., and Zhang, A.: Does lockdown reduce air pollution? Evidence from 44 cities in
514 northern China, *Science of the Total Environment*, 731, 139052,
515 10.1016/j.scitotenv.2020.139052, 2020.
- 516 Cai, R., and Jiang, J.: A new balance formula to estimate new particle formation rate:
517 reevaluating the effect of coagulation scavenging, *Atmospheric Chemistry and Physics*, 17,
518 12659-12675, 10.5194/acp-17-12659-2017, 2017.
- 519 Cai, R., Yang, D., Fu, Y., Wang, X., Li, X., Ma, Y., Hao, J., Zheng, J., and Jiang, J.: Aerosol
520 surface area concentration: a governing factor in new particle formation in Beijing,
521 *Atmospheric Chemistry and Physics*, 17, 12327-12340, 10.5194/acp-17-12327-2017, 2017.
- 522 Cai, R., Yan, C., Worsnop, D. R., Bianchi, F., Kerminen, V.-M., Liu, Y., Wang, L., Zheng,
523 J., Kulmala, M., and Jiang, J.: An indicator for sulfuric acid-amine nucleation in atmospheric
524 environments, *Aerosol Science and Technology*, 55, 1059-1069,
525 10.1080/02786826.2021.1922598, 2021a.
- 526 Cai, R., Yan, C., Yang, D., Yin, R., Lu, Y., Deng, C., Fu, Y., Ruan, J., Li, X., Kontkanen, J.,
527 Zhang, Q., Kangasluoma, J., Ma, Y., Hao, J., Worsnop, D. R., Bianchi, F., Paasonen, P.,
528 Kerminen, V. M., Liu, Y., Wang, L., Zheng, J., Kulmala, M., and Jiang, J.: Sulfuric acid-
529 amine nucleation in urban Beijing, *Atmospheric Chemistry and Physics*, 21, 2457-2468,
530 10.5194/acp-21-2457-2021, 2021b.
- 531 Chu, B., Zhang, S., Liu, J., Ma, Q., and He, H.: Significant concurrent decrease in PM_{2.5} and
532 NO₂ concentrations in China during COVID-19 epidemic, *Journal of Environmental
533 Sciences (China)*, 99, 346-353, 10.1016/j.jes.2020.06.031, 2021.
- 534 Ciarelli, G., Jiang, J., El Haddad, I., Bigi, A., Aksoyoglu, S., Prévôt, A. S. H., Marinoni, A.,
535 Shen, J., Yan, C., and Bianchi, F.: Modeling the effect of reduced traffic due to COVID-19
536 measures on air quality using a chemical transport model: impacts on the Po Valley and the
537 Swiss Plateau regions, *Environmental Science: Atmospheres*, 1, 228-240,
538 10.1039/D1EA00036E, 2021.
- 539 Dal Maso, M., Kulmala, M., Riipinen, I., Wagner, R., Hussein, T., Aalto, P. P., and Lehtinen,
540 K. E.: Formation and growth of fresh atmospheric aerosols: eight years of aerosol size



- 541 distribution data from SMEAR II, Hyytiälä, Finland, *Boreal Environment Research*, 10, 323-
542 336, 2005.
- 543 Deng, C., Fu, Y., Dada, L., Yan, C., Cai, R., Yang, D., Zhou, Y., Yin, R., Lu, Y., Li, X.,
544 Qiao, X., Fan, X., Nie, W., Kontkanen, J., Kangasluoma, J., Chu, B., Ding, A., Kerminen, V.
545 M., Paasonen, P., Worsnop, D. R., Bianchi, F., Liu, Y., Zheng, J., Wang, L., Kulmala, M.,
546 and Jiang, J.: Seasonal Characteristics of New Particle Formation and Growth in Urban
547 Beijing, *Environmental Science & Technology*, 54, 8547-8557, 10.1021/acs.est.0c00808,
548 2020.
- 549 Deng, C., Cai, R., Yan, C., Zheng, J., and Jiang, J.: Formation and growth of sub-3 nm
550 particles in megacities: impact of background aerosols, *Faraday Discussion*, 226, 348-363,
551 10.1039/d0fd00083c, 2021.
- 552 Ehn, M., Thornton, J. A., Kleist, E., Sipila, M., Junninen, H., Pullinen, I., Springer, M.,
553 Rubach, F., Tillmann, R., Lee, B., Lopez-Hilfiker, F., Andres, S., Acir, I. H., Rissanen, M.,
554 Jokinen, T., Schobesberger, S., Kangasluoma, J., Kontkanen, J., Nieminen, T., Kurten, T.,
555 Nielsen, L. B., Jorgensen, S., Kjaergaard, H. G., Canagaratna, M., Maso, M. D., Berndt, T.,
556 Petaja, T., Wahner, A., Kerminen, V. M., Kulmala, M., Worsnop, D. R., Wildt, J., and
557 Mentel, T. F.: A large source of low-volatility secondary organic aerosol, *Nature*, 506, 476-
558 479, 10.1038/nature13032, 2014.
- 559 Garmash, O., Rissanen, M. P., Pullinen, I., Schmitt, S., Kausiala, O., Tillmann, R., Zhao, D.,
560 Percival, C., Bannan, T. J., Priestley, M., Hallquist, Å. M., Kleist, E., Kiendler-Scharr, A.,
561 Hallquist, M., Berndt, T., McFiggans, G., Wildt, J., Mentel, T. F., and Ehn, M.: Multi-
562 generation OH oxidation as a source for highly oxygenated organic molecules from
563 aromatics, *Atmospheric Chemistry and Physics*, 20, 515-537, 10.5194/acp-20-515-2020,
564 2020.
- 565 Guo, S., Hu, M., Zamora, M. L., Peng, J., Shang, D., Zheng, J., Du, Z., Wu, Z., Shao, M.,
566 Zeng, L., Molina, M. J., and Zhang, R.: Elucidating severe urban haze formation in China,
567 *Proceedings of the National Academy of Sciences U S A*, 111, 17373-17378,
568 10.1073/pnas.1419604111, 2014.
- 569 Guo, S., Hu, M., Peng, J., Wu, Z., Zamora, M. L., Shang, D., Du, Z., Zheng, J., Fang, X.,
570 Tang, R., Wu, Y., Zeng, L., Shuai, S., Zhang, W., Wang, Y., Ji, Y., Li, Y., Zhang, A. L.,
571 Wang, W., Zhang, F., Zhao, J., Gong, X., Wang, C., Molina, M. J., and Zhang, R.:
572 Remarkable nucleation and growth of ultrafine particles from vehicular exhaust, *Proceedings*
573 *of the National Academy of Sciences U S A*, 117, 3427-3432, 10.1073/pnas.1916366117,
574 2020.
- 575 Harrison, R. M., Giorio, C., Beddows, D. C., and Dall'Osto, M.: Size distribution of airborne
576 particles controls outcome of epidemiological studies, *Science of the Total Environment*,
577 409, 289-293, 10.1016/j.scitotenv.2010.09.043, 2010.
- 578 Heinritzi, M., Simon, M., Steiner, G., Wagner, A. C., Kürten, A., Hansel, A., and Curtius, J.:
579 Characterization of the mass-dependent transmission efficiency of a CIMS, *Atmospheric*
580 *Measurement Techniques*, 9, 1449-1460, 10.5194/amt-9-1449-2016, 2016.



- 581 Huang, X., Ding, A., Gao, J., Zheng, B., Zhou, D., Qi, X., Tang, R., Wang, J., Ren, C., Nie,
582 W., Chi, X., Xu, Z., Chen, L., Li, Y., Che, F., Pang, N., Wang, H., Tong, D., Qin, W., Cheng,
583 W., Liu, W., Fu, Q., Liu, B., Chai, F., Davis, S. J., Zhang, Q., and He, K.: Enhanced
584 secondary pollution offset reduction of primary emissions during COVID-19 lockdown in
585 China, *National Science Review*, 8, 10.1093/nsr/nwaa137, 2021.
- 586 Kerminen, V.-M., and Kulmala, M.: Analytical formulae connecting the “real” and the
587 “apparent” nucleation rate and the nuclei number concentration for atmospheric nucleation
588 events, *Journal of Aerosol Science*, 33, 609-622, 10.1016/s0021-8502(01)00194-x, 2002.
- 589 Krecl, P., Targino, A. C., Oukawa, G. Y., and Cassino Junior, R. P.: Drop in urban air
590 pollution from COVID-19 pandemic: Policy implications for the megacity of Sao Paulo,
591 *Environmental Pollution*, 265, 114883, 10.1016/j.envpol.2020.114883, 2020.
- 592 Kulmala, M., Petaja, T., Nieminen, T., Sipila, M., Manninen, H. E., Lehtipalo, K., Dal Maso,
593 M., Aalto, P. P., Junninen, H., Paasonen, P., Riipinen, I., Lehtinen, K. E., Laaksonen, A., and
594 Kerminen, V. M.: Measurement of the nucleation of atmospheric aerosol particles, *Nature*
595 *Protocols*, 7, 1651-1667, 10.1038/nprot.2012.091, 2012.
- 596 Kulmala, M., Petaja, T., Ehn, M., Thornton, J., Sipila, M., Worsnop, D. R., and Kerminen, V.
597 M.: Chemistry of atmospheric nucleation: on the recent advances on precursor
598 characterization and atmospheric cluster composition in connection with atmospheric new
599 particle formation, *Annual Review of Physical Chemistry*, 65, 21-37, 10.1146/annurev-
600 physchem-040412-110014, 2014.
- 601 Kulmala, M., Kerminen, V. M., Petaja, T., Ding, A. J., and Wang, L.: Atmospheric gas-to-
602 particle conversion: why NPF events are observed in megacities?, *Faraday Discussion*, 200,
603 271-288, 10.1039/c6fd00257a, 2017.
- 604 Kulmala, M., Dada, L., Daellenbach, K. R., Yan, C., Stolzenburg, D., Kontkanen, J., Ezhova,
605 E., Hakala, S., Tuovinen, S., Kokkonen, T. V., Kurppa, M., Cai, R., Zhou, Y., Yin, R.,
606 Baalbaki, R., Chan, T., Chu, B., Deng, C., Fu, Y., Ge, M., He, H., Heikkinen, L., Junninen,
607 H., Liu, Y., Lu, Y., Nie, W., Rusanen, A., Vakkari, V., Wang, Y., Yang, G., Yao, L., Zheng,
608 J., Kujansuu, J., Kangasluoma, J., Petaja, T., Paasonen, P., Jarvi, L., Worsnop, D., Ding, A.,
609 Liu, Y., Wang, L., Jiang, J., Bianchi, F., and Kerminen, V. M.: Is reducing new particle
610 formation a plausible solution to mitigate particulate air pollution in Beijing and other
611 Chinese megacities?, *Faraday Discussion*, 226, 334-347, 10.1039/d0fd00078g, 2021.
- 612 Kurten, A., Rondo, L., Ehrhart, S., and Curtius, J.: Calibration of a chemical ionization mass
613 spectrometer for the measurement of gaseous sulfuric acid, *Journal of Physical Chemistry A*,
614 116, 6375-6386, 10.1021/jp212123n, 2012.
- 615 Kurten, A., Jokinen, T., Simon, M., Sipila, M., Sarnela, N., Junninen, H., Adamov, A.,
616 Almeida, J., Amorim, A., Bianchi, F., Breitenlechner, M., Dommen, J., Donahue, N. M.,
617 Duplissy, J., Ehrhart, S., Flagan, R. C., Franchin, A., Hakala, J., Hansel, A., Heinritzi, M.,
618 Hutterli, M., Kangasluoma, J., Kirkby, J., Laaksonen, A., Lehtipalo, K., Leiminger, M.,
619 Makhmutov, V., Mathot, S., Onnela, A., Petaja, T., Praplan, A. P., Riccobono, F., Rissanen,
620 M. P., Rondo, L., Schobesberger, S., Seinfeld, J. H., Steiner, G., Tome, A., Trostl, J.,
621 Winkler, P. M., Williamson, C., Wimmer, D., Ye, P., Baltensperger, U., Carslaw, K. S.,
622 Kulmala, M., Worsnop, D. R., and Curtius, J.: Neutral molecular cluster formation of sulfuric



- 623 acid-dimethylamine observed in real time under atmospheric conditions, Proceedings of the
624 National Academy of Sciences U S A, 111, 15019-15024, 10.1073/pnas.1404853111, 2014.
- 625 Le, T., Wang, Y., Liu, L., Yang, J., Yung, Y. L., Li, G., and Seinfeld, J. H.: Unexpected air
626 pollution with marked emission reductions during the COVID-19 outbreak in China, Science,
627 369, 702, 10.1126/science.abb7431, 2020.
- 628 Lehtinen, K. E. J., Dal Maso, M., Kulmala, M., and Kerminen, V.-M.: Estimating nucleation
629 rates from apparent particle formation rates and vice versa: Revised formulation of the
630 Kerminen–Kulmala equation, Journal of Aerosol Science, 38, 988-994,
631 10.1016/j.jaerosci.2007.06.009, 2007.
- 632 Liu, Y., Yan, C., Feng, Z., Zheng, F., Fan, X., Zhang, Y., Li, C., Zhou, Y., Lin, Z., Guo, Y.,
633 Zhang, Y., Ma, L., Zhou, W., Liu, Z., Dada, L., Dällenbach, K., Kontkanen, J., Cai, R., Chan,
634 T., Chu, B., Du, W., Yao, L., Wang, Y., Cai, J., Kangasluoma, J., Kokkonen, T., Kujansuu,
635 J., Rusanen, A., Deng, C., Fu, Y., Yin, R., Li, X., Lu, Y., Liu, Y., Lian, C., Yang, D., Wang,
636 W., Ge, M., Wang, Y., Worsnop, D. R., Junninen, H., He, H., Kerminen, V.-M., Zheng, J.,
637 Wang, L., Jiang, J., Petäjä, T., Bianchi, F., and Kulmala, M.: Continuous and comprehensive
638 atmospheric observations in Beijing: a station to understand the complex urban atmospheric
639 environment, Big Earth Data, 4, 295-321, 10.1080/20964471.2020.1798707, 2020.
- 640 Molteni, U., Bianchi, F., Klein, F., El Haddad, I., Frege, C., Rossi, M. J., Dommen, J., and
641 Baltensperger, U.: Formation of highly oxygenated organic molecules from aromatic
642 compounds, Atmospheric Chemistry and Physics, 18, 1909-1921, 10.5194/acp-18-1909-
643 2018, 2018.
- 644 Nieminen, T., Lehtinen, K. E. J., and Kulmala, M.: Sub-10 nm particle growth by vapor
645 condensation – effects of vapor molecule size and particle thermal speed, Atmospheric
646 Chemistry and Physics, 10, 9773-9779, 10.5194/acp-10-9773-2010, 2010.
- 647 Pei, Z., Han, G., Ma, X., Su, H., and Gong, W.: Response of major air pollutants to COVID-
648 19 lockdowns in China, Science of the Total Environment, 743, 140879,
649 10.1016/j.scitotenv.2020.140879, 2020.
- 650 Praske, E., Otkjaer, R. V., Crouse, J. D., Hethcox, J. C., Stoltz, B. M., Kjaergaard, H. G.,
651 and Wennberg, P. O.: Atmospheric autoxidation is increasingly important in urban and
652 suburban North America, Proceedings of the National Academy of Sciences U S A, 115, 64-
653 69, 10.1073/pnas.1715540115, 2018.
- 654 Qiao, X., Yan, C., Li, X., Guo, Y., Yin, R., Deng, C., Li, C., Nie, W., Wang, M., Cai, R.,
655 Huang, D., Wang, Z., Yao, L., Worsnop, D. R., Bianchi, F., Liu, Y., Donahue, N. M.,
656 Kulmala, M., and Jiang, J.: Contribution of Atmospheric Oxygenated Organic Compounds to
657 Particle Growth in an Urban Environment, Environmental Science & Technology,
658 10.1021/acs.est.1c02095, 2021.
- 659 Ronkko, T., Kuuluvainen, H., Karjalainen, P., Keskinen, J., Hillamo, R., Niemi, J. V., Pirjola,
660 L., Timonen, H. J., Saarikoski, S., Saukko, E., Jarvinen, A., Silvennoinen, H., Rostedt, A.,
661 Olin, M., Yli-Ojanpera, J., Nousiainen, P., Koussa, A., and Dal Maso, M.: Traffic is a major
662 source of atmospheric nanocluster aerosol, Proceedings of the National Academy of Sciences
663 U S A, 114, 7549-7554, 2017.



- 664 Shen, J., Bigi, A., Marinoni, A., Lampilahti, J., Kontkanen, J., Ciarelli, G., Putaud, J. P.,
665 Nieminen, T., Kulmala, M., Lehtipalo, K., and Bianchi, F.: Emerging Investigator Series:
666 COVID-19 lockdown effects on aerosol particle size distributions in northern Italy,
667 *Environmental Science: Atmospheres*, 1, 214-227, 10.1039/D1EA00016K, 2021a.
- 668 Shen, X., Sun, J., Yu, F., Wang, Y., Zhong, J., Zhang, Y., Hu, X., Xia, C., Zhang, S., and
669 Zhang, X.: Enhancement of nanoparticle formation and growth during the COVID-19
670 lockdown period in urban Beijing, *Atmospheric Chemistry and Physics*, 21, 7039-7052,
671 10.5194/acp-21-7039-2021, 2021b.
- 672 Shi, X., and Brasseur, G. P.: The Response in Air Quality to the Reduction of Chinese
673 Economic Activities During the COVID-19 Outbreak, *Geophysical Research Letters*, 47,
674 e2020GL088070, 10.1029/2020GL088070, 2020.
- 675 Sicard, P., De Marco, A., Agathokleous, E., Feng, Z., Xu, X., Paoletti, E., Rodriguez, J. J. D.,
676 and Calatayud, V.: Amplified ozone pollution in cities during the COVID-19 lockdown,
677 *Science of the Total Environment*, 735, 139542, 10.1016/j.scitotenv.2020.139542, 2020.
- 678 Stolzenburg, D., Fischer, L., Vogel, A. L., Heinritzi, M., Schervish, M., Simon, M., Wagner,
679 A. C., Dada, L., Ahonen, L. R., Amorim, A., Baccarini, A., Bauer, P. S., Baumgartner, B.,
680 Bergen, A., Bianchi, F., Breitenlechner, M., Brilke, S., Buenrostro Mazon, S., Chen, D., Dias,
681 A., Draper, D. C., Duplissy, J., El Haddad, I., Finkenzeller, H., Frege, C., Fuchs, C.,
682 Garmash, O., Gordon, H., He, X., Helm, J., Hofbauer, V., Hoyle, C. R., Kim, C., Kirkby, J.,
683 Kontkanen, J., Kurten, A., Lampilahti, J., Lawler, M., Lehtipalo, K., Leiminger, M., Mai, H.,
684 Mathot, S., Mentler, B., Molteni, U., Nie, W., Nieminen, T., Nowak, J. B., Ojdanic, A.,
685 Onnela, A., Passananti, M., Petaja, T., Quelever, L. L. J., Rissanen, M. P., Sarnela, N.,
686 Schallhart, S., Tauber, C., Tome, A., Wagner, R., Wang, M., Weitz, L., Wimmer, D., Xiao,
687 M., Yan, C., Ye, P., Zha, Q., Baltensperger, U., Curtius, J., Dommen, J., Flagan, R. C.,
688 Kulmala, M., Smith, J. N., Worsnop, D. R., Hansel, A., Donahue, N. M., and Winkler, P. M.:
689 Rapid growth of organic aerosol nanoparticles over a wide tropospheric temperature range,
690 *Proceedings of the National Academy of Sciences U S A*, 115, 9122-9127,
691 10.1073/pnas.1807604115, 2018.
- 692 Stolzenburg, D., Simon, M., Ranjithkumar, A., Kürten, A., Lehtipalo, K., Gordon, H.,
693 Ehrhart, S., Finkenzeller, H., Pichelstorfer, L., Nieminen, T., He, X.-C., Brilke, S., Xiao, M.,
694 Amorim, A., Baalbaki, R., Baccarini, A., Beck, L., Bräkling, S., Caudillo Murillo, L., Chen,
695 D., Chu, B., Dada, L., Dias, A., Dommen, J., Duplissy, J., El Haddad, I., Fischer, L.,
696 Gonzalez Carracedo, L., Heinritzi, M., Kim, C., Koenig, T. K., Kong, W., Lamkaddam, H.,
697 Lee, C. P., Leiminger, M., Li, Z., Makhmutov, V., Manninen, H. E., Marie, G., Marten, R.,
698 Müller, T., Nie, W., Partoll, E., Petäjä, T., Pfeifer, J., Philippov, M., Rissanen, M. P., Rörup,
699 B., Schobesberger, S., Schuchmann, S., Shen, J., Sipilä, M., Steiner, G., Stozhkov, Y.,
700 Tauber, C., Tham, Y. J., Tomé, A., Vazquez-Puffleau, M., Wagner, A. C., Wang, M., Wang,
701 Y., Weber, S. K., Wimmer, D., Wlasits, P. J., Wu, Y., Ye, Q., Zauner-Wieczorek, M.,
702 Baltensperger, U., Carslaw, K. S., Curtius, J., Donahue, N. M., Flagan, R. C., Hansel, A.,
703 Kulmala, M., Lelieveld, J., Volkamer, R., Kirkby, J., and Winkler, P. M.: Enhanced growth
704 rate of atmospheric particles from sulfuric acid, *Atmospheric Chemistry and Physics*, 20,
705 7359-7372, 10.5194/acp-20-7359-2020, 2020.
- 706 Trostl, J., Chuang, W. K., Gordon, H., Heinritzi, M., Yan, C., Molteni, U., Ahlm, L., Frege,
707 C., Bianchi, F., Wagner, R., Simon, M., Lehtipalo, K., Williamson, C., Craven, J. S.,



- 708 Duplissy, J., Adamov, A., Almeida, J., Bernhammer, A. K., Breitenlechner, M., Brilke, S.,
709 Dias, A., Ehrhart, S., Flagan, R. C., Franchin, A., Fuchs, C., Guida, R., Gysel, M., Hansel, A.,
710 Hoyle, C. R., Jokinen, T., Junninen, H., Kangasluoma, J., Keskinen, H., Kim, J., Krapf, M.,
711 Kurten, A., Laaksonen, A., Lawler, M., Leiminger, M., Mathot, S., Mohler, O., Nieminen, T.,
712 Onnela, A., Petaja, T., Piel, F. M., Miettinen, P., Rissanen, M. P., Rondo, L., Sarnela, N.,
713 Schobesberger, S., Sengupta, K., Sipila, M., Smith, J. N., Steiner, G., Tome, A., Virtanen, A.,
714 Wagner, A. C., Weingartner, E., Wimmer, D., Winkler, P. M., Ye, P., Carslaw, K. S.,
715 Curtius, J., Dommen, J., Kirkby, J., Kulmala, M., Riipinen, I., Worsnop, D. R., Donahue, N.
716 M., and Baltensperger, U.: The role of low-volatility organic compounds in initial particle
717 growth in the atmosphere, *Nature*, 533, 527-531, 10.1038/nature18271, 2016.
- 718 Wang, M., Kong, W., Marten, R., He, X.-C., Chen, D., Pfeifer, J., Heitto, A., Kontkanen, J.,
719 Dada, L., Kürten, A., Yli-Juuti, T., Manninen, H. E., Amanatidis, S., Amorim, A., Baalbaki,
720 R., Baccarini, A., Bell, D. M., Bertozzi, B., Bräkling, S., Brilke, S., Murillo, L. C., Chiu, R.,
721 Chu, B., De Menezes, L.-P., Duplissy, J., Finkenzeller, H., Carracedo, L. G., Granzin, M.,
722 Guida, R., Hansel, A., Hofbauer, V., Krechmer, J., Lehtipalo, K., Lamkaddam, H.,
723 Lampimäki, M., Lee, C. P., Makhmutov, V., Marie, G., Mathot, S., Mauldin, R. L., Mentler,
724 B., Müller, T., Onnela, A., Partoll, E., Petäjä, T., Philippov, M., Pospisilova, V.,
725 Ranjithkumar, A., Rissanen, M., Rörup, B., Scholz, W., Shen, J., Simon, M., Sipilä, M.,
726 Steiner, G., Stolzenburg, D., Tham, Y. J., Tomé, A., Wagner, A. C., Wang, D. S., Wang, Y.,
727 Weber, S. K., Winkler, P. M., Wlasits, P. J., Wu, Y., Xiao, M., Ye, Q., Zauner-Wieczorek,
728 M., Zhou, X., Volkamer, R., Riipinen, I., Dommen, J., Curtius, J., Baltensperger, U.,
729 Kulmala, M., Worsnop, D. R., Kirkby, J., Seinfeld, J. H., El-Haddad, I., Flagan, R. C., and
730 Donahue, N. M.: Rapid growth of new atmospheric particles by nitric acid and ammonia
731 condensation, *Nature*, 581, 184-189, 10.1038/s41586-020-2270-4, 2020a.
- 732 Wang, P., Chen, K., Zhu, S., Wang, P., and Zhang, H.: Severe air pollution events not
733 avoided by reduced anthropogenic activities during COVID-19 outbreak, *Resour Conserv*
734 *Recycl*, 158, 104814, 10.1016/j.resconrec.2020.104814, 2020b.
- 735 Wang, S., Wu, R., Berndt, T., Ehn, M., and Wang, L.: Formation of Highly Oxidized
736 Radicals and Multifunctional Products from the Atmospheric Oxidation of Alkylbenzenes,
737 *Environ Sci Technol*, 51, 8442-8449, 10.1021/acs.est.7b02374, 2017.
- 738 Xiao, M., Hoyle, C. R., Dada, L., Stolzenburg, D., Kürten, A., Wang, M., Lamkaddam, H.,
739 Garmash, O., Mentler, B., Molteni, U., Baccarini, A., Simon, M., He, X.-C., Lehtipalo, K.,
740 Ahonen, L. R., Baalbaki, R., Bauer, P. S., Beck, L., Bell, D., Bianchi, F., Brilke, S., Chen, D.,
741 Chiu, R., Dias, A., Duplissy, J., Finkenzeller, H., Gordon, H., Hofbauer, V., Kim, C., Koenig,
742 T. K., Lampilahti, J., Lee, C. P., Li, Z., Mai, H., Makhmutov, V., Manninen, H. E., Marten,
743 R., Mathot, S., Mauldin, R. L., Nie, W., Onnela, A., Partoll, E., Petäjä, T., Pfeifer, J.,
744 Pospisilova, V., Quéléver, L. L. J., Rissanen, M., Schobesberger, S., Schuchmann, S.,
745 Stozhkov, Y., Tauber, C., Tham, Y. J., Tomé, A., Vazquez-Pufleau, M., Wagner, A. C.,
746 Wagner, R., Wang, Y., Weitz, L., Wimmer, D., Wu, Y., Yan, C., Ye, P., Ye, Q., Zha, Q.,
747 Zhou, X., Amorim, A., Carslaw, K., Curtius, J., Hansel, A., Volkamer, R., Winkler, P. M.,
748 Flagan, R. C., Kulmala, M., Worsnop, D. R., Kirkby, J., Donahue, N. M., Baltensperger, U.,
749 El Haddad, I., and Dommen, J.: The driving factors of new particle formation and growth in
750 the polluted boundary layer, *Atmospheric Chemistry and Physics*, 21, 14275-14291,
751 10.5194/acp-21-14275-2021, 2021.



752 Xing, J., Li, S., Jiang, Y., Wang, S., Ding, D., Dong, Z., Zhu, Y., and Hao, J.: Quantifying the
753 emission changes and associated air quality impacts during the COVID-19 pandemic on the
754 North China Plain: a response modeling study, *Atmospheric Chemistry and Physics*, 20,
755 14347-14359, 10.5194/acp-20-14347-2020, 2020.

756 Yan, C., Nie, W., Vogel, A. L., Dada, L., Lehtipalo, K., Stolzenburg, D., Wagner, R.,
757 Rissanen, M. P., Xiao, M., Ahonen, L., Fischer, L., Rose, C., Bianchi, F., Gordon, H., Simon,
758 M., Heinritzi, M., Garmash, O., Roldin, P., Dias, A., Ye, P., Hofbauer, V., Amorim, A.,
759 Bauer, P. S., Bergen, A., Bernhammer, A. K., Breitenlechner, M., Brilke, S., Buchholz, A.,
760 Mazon, S. B., Canagaratna, M. R., Chen, X., Ding, A., Dommen, J., Draper, D. C., Duplissy,
761 J., Frege, C., Heyn, C., Guida, R., Hakala, J., Heikkinen, L., Hoyle, C. R., Jokinen, T.,
762 Kangasluoma, J., Kirkby, J., Kontkanen, J., Kurten, A., Lawler, M. J., Mai, H., Mathot, S.,
763 Mauldin, R. L., 3rd, Molteni, U., Niehman, L., Nieminen, T., Nowak, J., Ojdanic, A., Onnela,
764 A., Pajunoja, A., Petaja, T., Piel, F., Quelever, L. L. J., Sarnela, N., Schallhart, S., Sengupta,
765 K., Sipila, M., Tome, A., Trostl, J., Vaisanen, O., Wagner, A. C., Ylisirnio, A., Zha, Q.,
766 Baltensperger, U., Carslaw, K. S., Curtius, J., Flagan, R. C., Hansel, A., Riipinen, I., Smith, J.
767 N., Virtanen, A., Winkler, P. M., Donahue, N. M., Kerminen, V. M., Kulmala, M., Ehn, M.,
768 and Worsnop, D. R.: Size-dependent influence of NO_x on the growth rates of organic aerosol
769 particles, *Science Advances*, 6, eaay4945, 10.1126/sciadv.aay4945, 2020.

770 Yan, C., Yin, R., Lu, Y., Dada, L., Yang, D., Fu, Y., Kontkanen, J., Deng, C., Garmash, O.,
771 Ruan, J., Baalbaki, R., Schervish, M., Cai, R., Bloss, M., Chan, T., Chen, T., Chen, Q., Chen,
772 X., Chen, Y., Chu, B., Dällenbach, K., Foreback, B., He, X., Heikkinen, L., Jokinen, T.,
773 Junninen, H., Kangasluoma, J., Kokkonen, T., Kurppa, M., Lehtipalo, K., Li, H., Li, H., Li,
774 X., Liu, Y., Ma, Q., Paasonen, P., Rantala, P., Pileci, R. E., Rusanen, A., Sarnela, N.,
775 Simonen, P., Wang, S., Wang, W., Wang, Y., Xue, M., Yang, G., Yao, L., Zhou, Y.,
776 Kujansuu, J., Petäjä, T., Nie, W., Ma, Y., Ge, M., He, H., Donahue, N. M., Worsnop, D. R.,
777 Kerminen, V.-M., Wang, L., Liu, Y., Zheng, J., Kulmala, M., Jiang, J., and Bianchi, F.: The
778 Synergistic Role of Sulfuric Acid, Bases, and Oxidized Organics Governing New-Particle
779 Formation in Beijing, *Geophysical Research Letters*, 48, e2020GL091944,
780 <https://doi.org/10.1029/2020GL091944>, 2021.

781 Yao, L., Garmash, O., Bianchi, F., Zheng, J., Yan, C., Kontkanen, J., Junninen, H., Mazon, S.
782 B., Ehn, M., Paasonen, P., Sipilä, M., Wang, M., Wang, X., Xiao, S., Chen, H., Lu, Y.,
783 Zhang, B., Wang, D., Fu, Q., Geng, F., Li, L., Wang, H., Qiao, L., Yang, X., Chen, J.,
784 Kerminen, V.-M., Petäjä, T., Worsnop, D. R., Kulmala, M., and Wang, L.: Atmospheric new
785 particle formation from sulfuric acid and amines in a Chinese megacity, *Science*, 361, 278-
786 281, 10.1126/science.aao4839, 2018.

787 Yin, R., Yan, C., Cai, R., Li, X., Shen, J., Lu, Y., Schobesberger, S., Fu, Y., Deng, C., Wang,
788 L., Liu, Y., Zheng, J., Xie, H., Bianchi, F., Worsnop, D. R., Kulmala, M., and Jiang, J.: Acid-
789 Base Clusters during Atmospheric New Particle Formation in Urban Beijing, *Environmental
790 Science & Technology*, 55, 10994-11005, 10.1021/acs.est.1c02701, 2021.

791 Zhao, Y., Saleh, R., Saliba, G., Presto, A. A., Gordon, T. D., Drozd, G. T., Goldstein, A. H.,
792 Donahue, N. M., and Robinson, A. L.: Reducing secondary organic aerosol formation from
793 gasoline vehicle exhaust, *Proceedings of the National Academy of Sciences U S A*, 114,
794 6984, 10.1073/pnas.1620911114, 2017.

795